

# The simulation of non-Hermitian disordered system in linear circuits

Luhong Su,<sup>1,2</sup> Hui Jiang,<sup>3,\*</sup> Zhan Wang,<sup>1,2</sup> Shu Chen,<sup>1,4,5,†</sup> and Dongning Zheng<sup>1,4,6,‡</sup>

<sup>1</sup>*Beijing National Laboratory for Condensed Matter Physics,  
Institute of Physics, Chinese Academy of Sciences, Beijing 100190, China*

<sup>2</sup>*School of Physical Sciences, University of Chinese Academy of Sciences, Beijing 100049, China*

<sup>3</sup>*Department of Physics, National University of Singapore, Singapore 117542*

<sup>4</sup>*CAS Center for Excellence in Topological Quantum Computation and School of Physical Sciences,  
University of Chinese Academy of Sciences, Beijing 100049, China*

<sup>5</sup>*The Yangtze River Delta Physics Research Center, Liyang, Jiangsu 213300, China*

<sup>6</sup>*Songshan Lake Materials Laboratory, Dongguan, Guangdong 523808, China*

Non-Hermitian skin effect (NHSE) is a novel phenomenon appearing in non-Hermitian systems. Here, we report the experimental observation of NHSE. Different from the previous non-reciprocal circuit implementation scheme using logic components, we construct our one-dimensional (1D) circuits using linear components only. Besides, we achieve the non-reciprocity by proportionally varying the parameter value of the components. By measuring the voltage response of each site, the information of eigenstates can be mapped out. The results show that the voltage response is always larger on one end of the circuit no matter on which end voltage driving is applied, indicating clearly the presence of the NHSE. Furthermore, we also simulate the interplay of NHSE and Anderson localization (AL) when additional disorder is introduced. Upon increasing the disorder strength, we observe the transformation from the skin effect phase to the localized phase. In the regime of skin effect phase, the eigenstates are all localized at one edge while eigenstates are affected by the voltage supply input in localized phase. Our findings unveil a possible new route for simulation of topological phenomena in non-Hermitian systems.

## I. INTRODUCTION

While the Hamiltonian of a closed quantum system is always Hermitian, it has been demonstrated that some open quantum systems, optic systems and electric circuits can be effectively modeled by non-Hermitian Hamiltonians<sup>1</sup>. Non-Hermitian systems have been unveiled to exhibit some unique features, such as non-Hermitian skin effect (NHSE), which is characterized by the accumulation of a majority of eigenstates on the boundaries<sup>2,3</sup>. To date, the NHSE has been extensively investigated from various theoretical aspects<sup>4–18</sup>.

The theoretical progress has further promoted experimental studies on the properties of non-Hermitian systems<sup>19–23</sup>, which have been performed in optical field<sup>24–26</sup>, micro-resonator<sup>27</sup>, cold atom<sup>28</sup>, robotic metamaterials<sup>29,30</sup> and electric circuits<sup>31</sup>. The non-Hermitian system with NHSE is sensitive to boundary conditions<sup>14,32</sup>. When the boundary condition of the system changes from the periodic boundary to open boundary, the energy spectrum of the system changes drastically, which reflects the boundary sensitivity of the skin effect. Due to the design flexibility and simplicity, electric circuits have become a powerful platform for studying topological effects in recent years<sup>33–39</sup>. Some topological phenomena have been demonstrated<sup>33</sup>, such as the boundary states with topological protection in the one-dimensional SSH model<sup>34–38</sup>, the generalized Brillouin zone and the generalized bulk boundary correspondence<sup>40,41</sup>, the high-order topological state in high-dimensional lattice circuits<sup>36,42</sup>. Majority of the circuit design realizes non-Hermiticity relying on using active devices<sup>40,41,43–47</sup>. The simplest model exhibiting the

NHSE is the Hatano-Nelson (HN) model<sup>48,49</sup>, which can be realized by generating non-reciprocal hopping. However, this has not been demonstrated experimentally in RLC linear electric circuit without any logic devices.

Using the platform of RLC linear electric circuit, we can realize the non-Hermitian system with non-reciprocal hopping and study the topological phase transition induced by the competition of non-reciprocal hopping and disorder. NHSE is characterized by the emergence of bulk eigenstates localized in the boundary due to the regular unidirectional gain or loss during the transmission of electronic waves between lattice points. In contrast, if the electron wave is perturbed randomly, the wave function of the electron will be confined to a certain range and no longer propagate, which is known as the Anderson localization (AL)<sup>50,51</sup>. The similarities and differences between the two phenomena have received attentions. An interesting issue is how the wave function behaves if the particle is subjected to both regular unidirectional gain and random perturbation? And what will the wave function be? Recently the interplay of NHSE and AL has been studied theoretically by considering the non-reciprocal quasiperiodic model<sup>52</sup>, which stimulates intensive theoretical interest on the study of localization phenomena in non-reciprocal systems<sup>53–55</sup>. However, experimental study on this interesting issue is still lacking. In this paper, we address the above issue in the RLC linear electric circuit with non-reciprocal hopping.

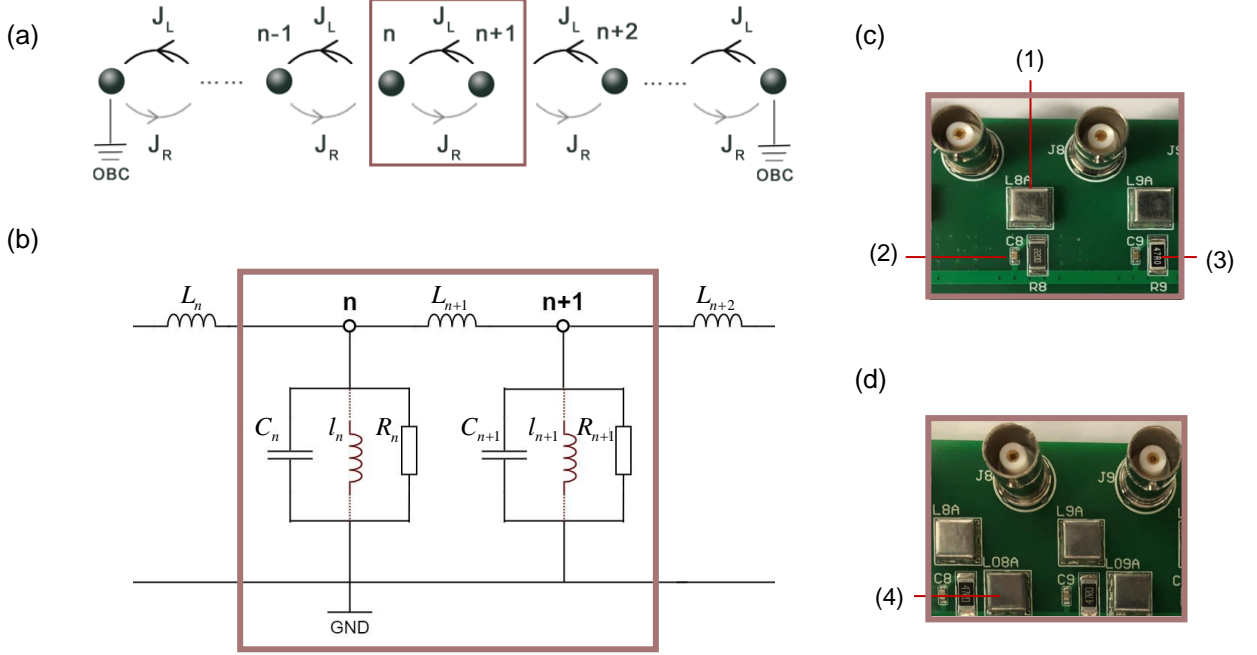


FIG. 1: Reciprocity breaking in a non-Hermitian linear RLC circuit. (a) Schematic diagram of non-reciprocal one-band hopping model, where  $J_{R(L)}$  is the right(left)-hopping amplitude. (b) Experimental implementation of a non-reciprocal circuit model based on Fig. 1(a). The asymmetrical couplings are achieved by ratio of two adjacent inductors  $L_n = Lg^{-n}$ . The  $\gamma$  term is achieved by the resistors. The brown dotted line represents the on site potential, which divides the samples into one-band non-Hermitian system Fig. 1(c) and the interplay system Fig. 1(d). The numbers label the circuit components: (1) surface mounted device (SMD) inductor; (2) SMD capacitor ( $C_n \approx Cg^n$ ); (3) SMD resistor ( $R_n = Rg^{-n}$ ), (4) additional SMD inductor in interplay system:  $\Delta_n = L_n/l_n$ , left-skin phase:  $J_L = g = 2.2$ ,  $\Delta_n$  random select in  $[7 \times 10^{-5}, 0.33]$ , localized phase:  $J_L = g = 2.2$ ,  $\Delta_n = 2\Delta \cos(2\pi\beta n)$ ,  $\beta = (\sqrt{5} - 1)/2$ .

## II. NON-RECIPROCITY CIRCUIT

In this work, we choose the HN model to exhibit the NHSE experimentally. The model is illustrated schematically in Fig. 1(a), where  $J_{R(L)}$  is the right (left)-hopping amplitude and  $J_R \neq J_L$ . The Hamiltonian of the model can be written as:

$$H = \sum_n J_R |n+1\rangle \langle n| + J_L |n\rangle \langle n+1|. \quad (1)$$

To simulate this model, we construct a chain circuit that consists of 10 unit-cells using linear components (such as capacitors and inductors) only. Obviously, non-reciprocity cannot be achieved by simply using the same repeating unit. Instead, we build the circuit with capacitance and inductance of each unit vary proportionally at a constant ratio  $g$ , as suggested in Ref. <sup>52</sup>. According to Kirchhoff's law, for the  $n$ th site, the voltage of adjacent unit-cells can be written as: (The details of the derivation are given in Appendix A.)

$$V_{n-1} + gV_{n+1} = (\omega^2/\omega_0^2 + 1 + g)V_n. \quad (2)$$

Eq. (2) can be described by the Hamiltonian Eq. (1) with  $J_R = 1$  and  $g = J_L/J_R$ . Hence, the behavior in HN model can be understood by investigating the voltage response of our system. In Fig. 1(b), we show two adjacent unit-cells of circuit. In each unit-cell, the brown inductor in parallel is used for the interplay system in section IV, and the resistors are used to stabilize the circuit. Capacitive and inductive elements achieve static equation  $\mathcal{H}\mathcal{V} = E\mathcal{V}$ , where  $\mathcal{H}$  is the matrix representation of the non-reciprocal Hamiltonian under the open boundary condition (OBC) and  $\mathcal{V} = (\dots, V_n, \dots)^T$ , as defined in Eq. (1). The eigenvalue  $E = \omega^2/\omega_0^2 + 1 + g$  and the parameter  $\omega_0 = 1/\sqrt{L_n C_n} = 1/\sqrt{LC}$  donates resonance frequency of single unit-cell. Therefore, we can obtain the information of eigenstates by measuring the voltage response at each site. However, the measurement of the static system requires a strong self-sustained energy gain, that is, after a short time of source feed, the voltage response can still be measured at each site respectively. But in the experiment the self-oscillating dissipation of the static system is strong, and the voltage decays rapidly.

Remarkably, dynamic measurements are more widely available in circuit experiments, so we introduce dynamic response. The information of the static equation can be obtained through the dynamic evolution equation when circuit is applied an alternating current (a.c.) voltage driving. The inhomogeneous equation with dimensionless parameters reads:

$$\frac{d^2}{d\tau^2}\mathcal{V}(\tau) - (\mathcal{H} - 1 - g)\mathcal{V}(\tau) = \mathcal{V}_e, \quad (3)$$

where  $\tau = \omega_0 t$  and  $\mathcal{V}_e$  donates the position of the external source  $V(f)$ , with  $\omega = 2\pi f$ . For example, if the a.c. voltage  $V(f)$  is imposed on the left side of the circuit, we have  $\mathcal{V}_e = (V(f), 0, \dots, 0)^T$ . The solution of Eq. (3) corresponds to the eigenstates of the  $\mathcal{H}$ . Thus, the distribution of the voltage response characterizes the eigenstates of the static equation.

In fact, Eq. (3) takes into account both the initial state and the first derivative of the initial state. While it is generally difficult to measure directly, we introduce the damping term into Eq. (3). We eventually arrive at a evolution equation:

$$\frac{d^2}{d\tau^2}\mathcal{V}(\tau) + \gamma \frac{d}{d\tau}\mathcal{V}(\tau) - (\mathcal{H} - 1 - g)\mathcal{V}(\tau) = \mathcal{V}_e, \quad (4)$$

where  $\gamma = (1/R)\sqrt{L/C}$ , with large values of resistance which is 20 times of the series inductance at the resonance frequency in our circuits, so that the system can stabilize quickly. The solution of Eq. (4) is :

$$\mathcal{V}(\tau) = e^{-\gamma\tau/2}\mathcal{V}_0(\tau) + \sum_n \mathcal{V}_n \mathcal{W}_n^T \mathcal{V}_e (a_n \cos\tilde{\Omega}t + b_n \sin\tilde{\Omega}t). \quad (5)$$

Here,  $\mathcal{V}_n$  and  $\mathcal{W}_n^T$  are  $n$ th right and left eigenvectors of  $\mathcal{H}$ . The  $\tilde{\Omega}$  means the frequency which is normalized to  $\omega_0$ .  $\mathcal{V}_0(\tau)$  is related to initial condition, and  $a_n(\tilde{\Omega}, \gamma)$ ,  $b_n(\tilde{\Omega}, \gamma) \in [-1, 1]$ . When  $\gamma \ll 1$ , the system is resonant with a large value of  $a_n$  and vanishing  $b_n$ , so the voltage response distribution of the system actually reflects the overlap of  $\mathcal{W}_n^T$  and  $\mathcal{V}_e$ .

By introducing resistance, the initial state can be ignored and the properties of the static system of the HN model can be obtained. The device parameters we use cover three orders of magnitude, which is completely different from the single repeating unit in traditional electric topology circuits reported in the literature<sup>33-39</sup>.

We fabricated a number of circuit boards with different  $g$  values. The total circuit configuration is shown in Fig. 2(b) where the dashed and dotted lines represent the left-side and right-side driving, respectively. The circuit elements of the unit-cell are specified in Fig. 1(b), while a physical unit cell board cutout is presented in Figs. 1(c) and 1(d).

### III. DYNAMIC MEASUREMENT

In this section, we give a more detailed description about the dynamic measurements and show the results.

During the experiment, we apply a.c. voltage  $V(f_n)$  to the left and to the right side respectively. Here,  $f_n$  is the resonance frequency of the system. By measuring the voltage response of each site, we can get the wave function distribution corresponding to the eigenenergy  $E_n$ . Firstly, we find out the resonance frequency by measuring the transmission coefficient of the system. The total system is treated as a two-ports device, through the equation:

$$\begin{pmatrix} V_1^- \\ V_2^- \end{pmatrix} = S \begin{pmatrix} V_1^+ \\ V_2^+ \end{pmatrix} = \begin{bmatrix} S_{11} & S_{12} \\ S_{21} & S_{22} \end{bmatrix} \begin{pmatrix} V_1^+ \\ V_2^+ \end{pmatrix}, \quad (6)$$

where  $V_i^{+/-}$  are the voltages of the incoming and outgoing signals at ports  $i$ , port 1 (2) is the left (right)-side of the circuit in Fig. 2(a), where  $S$  is the transmission coefficient matrix. The a.c. voltages are measured by a lock-in amplifier (Zurich Instruments UHF) working in the frequency scanning mode. The physical circuits for determining resonant frequency is shown in Fig. 2(a). We applied a voltage source drive at the port 1 (2), and measure the transmission response at each frequency at the port 2 (1). The Lorentz reciprocity theorem requires that the scattering matrix satisfies the symmetry condition  $S^T = S$ , so the signal transmission between two ports is the same for both propagation directions. For Hermitian system,  $S_{12} = S_{21}$ , so the left and right transfer functions are exactly the same. For the one-band non-reciprocal system,  $S_{12} \neq S_{21}$  results in the different transmission coefficients on the left and right and a port-dependent frequency shift. The transmission curve of Hermitian system is shown in Fig. 2(c), its imaginary part is plotted as a function of frequency  $f$ .

In electric circuits, the impedance of inductors and capacitors are  $Z_L = i2\pi fL$  and  $Z_C = -i/(2\pi fC)$  respectively, showing that inductors lead the phase while capacitors lag the phase. Therefore, in the transmission curve, the frequency of the point with zero imaginary part is the resonance frequency  $f_n$ . The Hermitian transmission curves are coincided completely, which are drastically different from the non-reciprocal transmission curves. For non-reciprocal systems, the voltage responses of  $S_{21}$  and  $S_{12}$  are very small due to the skin effect. Therefore, in the actual measurement, we use the resonance frequency  $f_n$  calculated theoretically.

As shown in Fig. 2(b), we apply a.c. voltage  $V(f_n)$  and measure the voltage response of each site, where  $V_{L(R)}$  is equal to port 1 (2) in Fig. 2(a). The results of the Hermitian system are shown in Fig. 2(d). Clearly, the curves of the voltage response obtained from Hermitian circuits look the same up to a left-right reflection, being consistent with the theoretical calculation that Hermitian systems exhibit extended states under OBCs. For Hermitian system, the wave functions are all extended states. Furthermore, the overlap of each extended state is similar, which meets  $\sum_n \mathcal{V}_n \times \mathcal{W}_n^T = 1$ , so that the voltage response reflects the information of the external source. The results in Fig. 2(d) shows that the voltage profile decreases with distance to the feed unit-cells. This is due

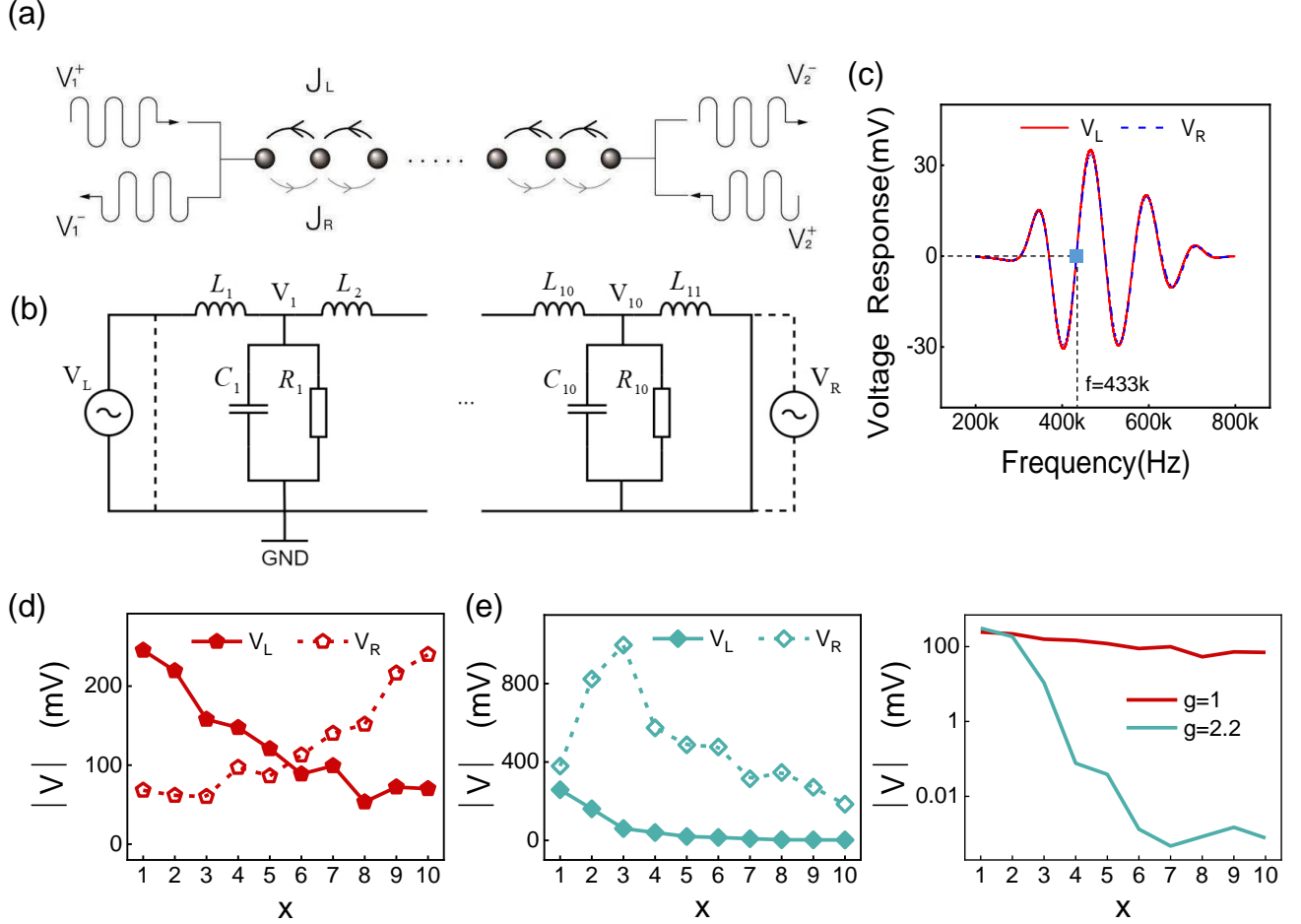


FIG. 2: (a) Schematic diagram of the measured transmission curve,  $V_i^{+/-}$  represents input/output a.c. voltage in right or left end. (b) A voltage source of a.c. driving  $f_n$  is imposed on the left or the right side of the circuit. We measure voltage response of 10 sites respectively. (c) Transmission curves of Hermitian extended state. The solid line is the imaginary part of  $S_{12}$  while the dotted line is  $S_{21}$  which show reciprocity,  $S_{12} = S_{21}$ , where  $S$  is the scattering matrix. The point with zero imaginary part is the resonance point, which is the eigenfrequency we choose. (d) Voltage response of each site in Hermitian extended state for input voltage a.c. frequency  $f = 433.0$  kHz. (e) Voltage response of each site in left-skin state for  $f = 260.8$  kHz. The voltage response all localized on the left boundary, and the right side voltage response is much higher than left side one. (f) Comparison chart of voltage response of  $g = 1$  vs.  $g = 2.2$  in left side voltage. We use logarithmic coordinates for ordinates.  $V_{L(R)}$  represent left (right) side Voltage in the Fig. 2 and Fig. 3.

to the presence of the resistors introduced for stabilizing dynamic measurements. Nevertheless, we see the voltage does not drop to very small value even for the 10th site, indicating the extended nature of the system.

In Fig. 2(e), we show the result with  $g = 2.2$ . Remarkably, our circuit produces a dominant voltage signal at the left edge whether the voltage feed is imposed on left or right side. When driving from left side,  $V_1$  is much larger than  $V_{10}$ , and  $V_1/V_{10} \approx 150$ . The voltage response rapidly decays to the right with the change of the position of the site, which fully reflects the skin effect that the eigenstates of the system are accumulated to the left boundary. When driving from right side, as shown in

Eq. (5), the overlap of  $W_n^T$  and  $V_e$  is very large which induces higher voltage response. Nevertheless, we can still see a trend of decreasing voltage from the left end to the right end, being consistent with the left skin effect.

So far, we have observed the NSHE. Meanwhile, for  $J_L > J_R$  ( $g = 2.2$ ) the corresponding system under periodic boundary condition is topologically nontrivial, which is characterized by the winding number  $w = -1$ . Whereas for  $J_L = J_R$  ( $g = 1$ ), the corresponding system is topologically trivial with  $w = 0$ <sup>10</sup>. The NSHE is characterized by the accumulation of eigenstates at the boundary. By comparing the skin states of the non-Hermitian system with the extended eigenstates of

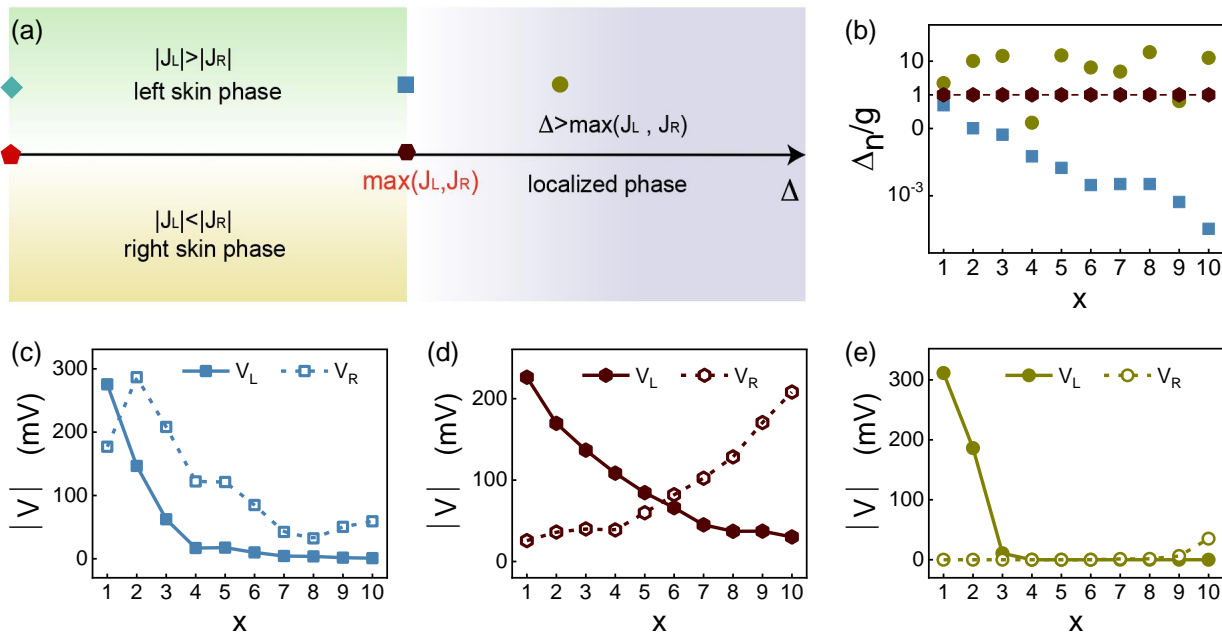


FIG. 3: (a) Phase diagram. The phase boundaries are determined by hopping amplitude  $|J_R|$  ( $|J_L|$ ) and disorder strength  $\Delta$ . Pentagon and diamond markers represent the parameters used in Fig. 2(c) and (d). The circle, hexagon and square markers correspond to localized phase, Hermitian phase and left-skin phase respectively and indicate the parameters used for (c)-(e). (b) Comparison of hopping coupling strength and disorder strength. (c) Voltage response of each site in left skin phase for  $f = 825.3$  kHz,  $J_L > J_R$  while disorder strength  $\Delta \approx 0.25$ . (d) Voltage response of each site in Hermitian case for  $f = 571.8$  kHz,  $J_L = J_R$  and  $\Delta_n = 1$ . (e) Voltage response of each site in localized phase for  $f = 1.82$  MHz,  $J_L > J_R$  while  $\Delta \approx 10$ .

the Hermitian system, we observe that the topologically different phases display quite different behaviors under the OBC. Remarkably, in our circuits, topological phase transitions can be realized by tuning the value of  $g$  even for a single-band lattice. In contrast, for Hermitian systems, at least two band systems (such as the SSH model) are required to observe topological phenomena. Furthermore, in a classical circuit, when a source is added, the voltage response gradually decreases along the loop, which is quite different from the NHSE in the non-reciprocal circuit.

#### IV. THE INTERPLAY OF NHSE AND AL

The NHSE can be achieved through a one-band non-reciprocal system, which is based on a simple hopping between the inductors and the capacitors. But the circuit platform by introducing tunable on-site potentials can simulate more complex systems. The circuit system can simulate the interplay of NHSE and AL when each site is connected with an inductor to form  $\Delta_n$  to act as a disorder term. When  $\Delta_n = 2\Delta \cos(2\pi\beta n)$ , the model becomes the non-reciprocal Aubry-André (AA) model where  $\Delta$  is the amplitude of the quasiperiodic potential and  $\beta$  takes the value of the golden ratio  $(\sqrt{5} - 1)/2$ . We arrive at

interplay system:

$$H = \sum_n J_R |n+1\rangle\langle n| + J_L |n\rangle\langle n+1| + \Delta_n |n\rangle\langle n|. \quad (7)$$

By adjusting the value of disorder strength  $\Delta_n$ , topological phase transition from skin phase to localized phase can be realized. Under the OBC, the non-reciprocal interplay model has three phases due to the competition between the AL and the NHSE. As shown in Fig. 3(a) and (b), corresponding to dominant term, there are three phases including left-skin phase, localized phase and right-skin phase. When the  $\Delta_n$  is small, the system is dominated by skin effect. Due to  $g > 1$ , system is in the left skin phase. Regardless of whether the source drive is added from the left or right, the voltage response is always localized on the left, as shown in Fig. 3(c). When the source is added from the left, the voltage response decays in turn,  $V_1/V_{10} \approx 100$ , similar to the non-Hermitian left skin state. However, when the source is added from the right, the left skin effect is further weakened, because small disorder is added to the system which compete with the skin effect. In this case, the hopping coupling strength is still much greater than the disorder strength, so the voltage response is all localized in the left boundary. It is worth noting that  $\Delta_n = L_n/l_n$  means that the selection of  $l_n$  should be as large as possible for the same

$L_n$ . As a reference, we design the Hermitian system of  $g = 1$ ,  $\Delta_n=1$ . In the Hermitian system, the transmission curves of the left and right ends are basically the same, and the voltage response of each site fluctuates less, as shown in the Fig. 3(d).

When disorder strength  $\Delta_n$  is further increased, the competition between localization and skin effect is strengthened, which can lead to a transition from skin phase to localized phase. When the average strength multiple of the localization is about 10 times of the hopping amplitudes, the skin phase is completely destroyed and the system is in the localized phase. When the source drive is added from the left end, the voltage response decreases rapidly from left to right  $V_1/V_{10} \approx 10^4$ . When the source drive is added from the right end, the voltage response decays from right to left,  $V_{10}/V_1 \approx 30$ , as shown in Fig. 3(e). In comparison with the left skin phase, non-reciprocal hopping still plays a role, but it is completely overwhelmed by the disorder strength.

Because the circuit of Printed Circuit Board (PCB) has inductance, when the cosine periodic potential is small, the inductance has a great influence on the circuit, resulting in the total system is still a localized phase. Therefore, for the parameter design of the left skin phase, the maximum  $l_n$  should be selected as large as possible. The three distinct phases are located at different locations in the phase diagram. For the left skin phase, although the skin effect is affected by the AL, the skin effect is still dominant. Phase transition occurs as the disorder becomes larger and dominant. For the localized phase, since the wave function is localized, it is insensitive to boundaries. Unlike the left skin phase, the voltage response is localized at the source of the added voltage, and the disorder results in attenuation as it gradually moves away from the source of the added voltage. The measurement process is similar to the non-reciprocal one-band model, for which the dynamic evolution is used to obtain the characteristics of the static system.

## V. CONCLUSION

In this paper, the NHSE is observed on a one-dimensional non-reciprocal one-band system with open boundary realized by linear electric circuits. Furthermore, this platform also simulates competition between disorder and skin effect, which leads to three different topological phases. When the disorder strength is small, the left skin phase is obtained. The voltage response is localized on the left whether the source is added from the left or the right side. When the the disorder strength is dominant, a dramatic change occurs, and the voltage response is localized on the side of the source. The skin effect is suppressed by the disorder term, but a great difference between the left and right end sources can still be observed. At this time, the system changes into the localized phase. We have successfully observed the characteristics of different phase regions.

Using linear circuits to simulate non-Hermitian phenomena is not only convenient, but also easy to operate. The measurement system is relatively easy to control, and the limitations of the environment are small. We have built the circuit with capacitance and inductance of each unit vary proportionally at a constant ratio  $g$  to realize non-reciprocity. We predict that it may provide a potential scheme for further research of critical skin effect in the future.

## ACKNOWLEDGMENTS

This work is supported by the State Key Development Program for Basic Research of China (Grant No. 2017YFA0304300), the Key-Area Research and Development Program of Guangdong Province, China (Grant No. 2020B0303030001), the National Natural Science Foundation of China (Grant No. T2121001, No. 12174436 and No. 11974413) and the Strategic Priority Research Program of Chinese Academy of Sciences (Grant No. XDB28000000).

---

\* Contributed equally to this work.

† Corresponding author: schen@iphy.ac.cn

‡ Corresponding author: dzheng@iphy.ac.cn

<sup>1</sup> Yuto Ashida, Zongping Gong, and Masahito Ueda, “Non-Hermitian physics,” *Adv. Phys.* **69**, 249 – 435 (2020).

<sup>2</sup> Tony E. Lee, “Anomalous edge state in a non-hermitian lattice,” *Phys. Rev. Lett.* **116**, 133903 (2016).

<sup>3</sup> Shunyu Yao and Zhong Wang, “Edge states and topological invariants of non-Hermitian systems,” *Phys. Rev. Lett.* **121**, 086803 (2018).

<sup>4</sup> Jong Yeon Lee, Junyeong Ahn, Hengyun Zhou, and Ashvin Vishwanath, “Topological correspondence between Hermitian and non-Hermitian systems: Anomalous dynamics,” *Phys. Rev. Lett.* **123**, 206404 (2019).

<sup>5</sup> Dimitrios L Sounas and Andrea Alù, “Non-reciprocal pho-

tonics based on time modulation,” *Nat. Photon.* **11**, 774–783 (2017).

<sup>6</sup> Pu Huang, Liang Zhang, Jingwei Zhou, Tian Tian, Peiran Yin, Changkui Duan, and Jiangfeng Du, “Nonreciprocal radio frequency transduction in a parametric mechanical artificial lattice,” *Phys. Rev. Lett.* **117**, 017701 (2016).

<sup>7</sup> Zhesen Yang, Kai Zhang, Chen Fang, and Jiangping Hu, “Non-Hermitian bulk-boundary correspondence and auxiliary generalized brillouin zone theory,” *Phys. Rev. Lett.* **125**, 226402 (2020).

<sup>8</sup> Stefano Longhi, “Probing non-Hermitian skin effect and non-bloch phase transitions,” *Phys. Rev. Res.* **1**, 023013 (2019).

<sup>9</sup> Dan S. Borgnia, Alex Jura Kruchkov, and Robert-Jan Slager, “Non-Hermitian boundary modes and topology,”

- Phys. Rev. Lett. **124**, 056802 (2020).
- 10 Zongping Gong, Yuto Ashida, Kohei Kawabata, Kazuaki Takasan, Sho Higashikawa, and Masahito Ueda, “Topological phases of non-Hermitian systems,” Phys. Rev. X **8**, 031079 (2018).
  - 11 Cem Yuce, “Eigenstate clustering around exceptional points,” Phys. Rev. A **102**, 032203 (2020).
  - 12 Guo-Qiang Zhang, Zhen Chen, Da Xu, Nathan Shammah, Meiyong Liao, Tie-Fu Li, Limin Tong, Shi-Yao Zhu, Franco Nori, and J. Q. You, “Exceptional point and cross-relaxation effect in a hybrid quantum system,” PRX Quantum **2**, 020307 (2021).
  - 13 Ling-Zhi Tang, Guo-Qing Zhang, Ling-Feng Zhang, and Dan-Wei Zhang, “Localization and topological transitions in non-Hermitian quasiperiodic lattices,” Phys. Rev. A **103**, 033325 (2021).
  - 14 Linhu Li, Ching Hua Lee, Sen Mu, and Jiangbin Gong, “Critical non-Hermitian skin effect,” Nat. Commun. **11**, 1–8 (2020).
  - 15 Chun-Hui Liu, Kai Zhang, Zhesen Yang, and Shu Chen, “Helical damping and dynamical critical skin effect in open quantum systems,” Phys. Rev. Res. **2**, 043167 (2020).
  - 16 Cem Yuce, “Nonlinear non-Hermitian skin effect,” Phys. Lett. A **408**, 127484 (2021).
  - 17 Ching Hua Lee, Linhu Li, Ronny Thomale, and Jiangbin Gong, “Unraveling non-Hermitian pumping: Emergent spectral singularities and anomalous responses,” Phys. Rev. B **102**, 085151 (2020).
  - 18 E. Prodan and H. Schulz-Baldes, “Bulk and boundary invariants for complex topological insulators: From k-theory to physics,” K (2016).
  - 19 Jiaming Li, Andrew K Harter, Ji Liu, Leonardo de Melo, Yogesh N Joglekar, and Le Luo, “Observation of parity-time symmetry breaking transitions in a dissipative floquet system of ultracold atoms,” Nat. Commun. **10**, 1–7 (2019).
  - 20 Shubo Wang, Bo Hou, Weixin Lu, Yuntian Chen, ZQ Zhang, and Che Ting Chan, “Arbitrary order exceptional point induced by photonic spin-orbit interaction in coupled resonators,” Nat. Commun. **10**, 1–9 (2019).
  - 21 Yang Wu, Wenquan Liu, Jianpei Geng, Xingrui Song, Xiangyu Ye, Chang-Kui Duan, Xing Rong, and Jiangfeng Du, “Observation of parity-time symmetry breaking in a single-spin system,” Science **364**, 878–880 (2019).
  - 22 Changqing Wang, William R. Sweeney, A. Douglas Stone, and Lan Yang, “Coherent perfect absorption at an exceptional point,” Science **373**, 1261 (2021).
  - 23 M. Naghiloo, M. Abbasi, Yogesh N., Joglekar, and K. W. Murch, “Quantum state tomography across the exceptional point in a single dissipative qubit,” Nat. Phys. **15**, 1232 (2019).
  - 24 Xueyi Zhu, Huaqiang Wang, Samit Kumar Gupta, Haijun Zhang, Biye Xie, Minghui Lu, and Yanfeng Chen, “Photonic non-Hermitian skin effect and non-bloch bulk-boundary correspondence,” Phys. Rev. Res. **2**, 013280 (2020).
  - 25 Tobias Helbig Tobias Hofmann Alexander Stegmaier Martin Greiter Ronny Thomale Sebastian Weidemann, Mark Kremer and Alexander Szameit, “Topological funneling of light,” Science **368**, 311–314 (2020).
  - 26 Lei Xiao, Tian-Shu Deng, Kunkun Wang, Gaoyan Zhu, Zhong Wang, Wei Yi, and Peng Xue, “Non-Hermitian bulkboundary correspondence in quantum dynamics,” Nat. Phys. **16**, 1–6 (2020).
  - 27 Lu Qi, Guo-Li Wang, Shutian Liu, Shou Zhang, and Hong-Fu Wang, “Robust interface-state laser in non-Hermitian microresonator arrays,” Phys. Rev. Appl. **13**, 064016 (2020).
  - 28 Linhu Li, Ching Hua Lee, and Jiangbin Gong, “Topological switch for non-Hermitian skin effect in cold-atom systems with loss,” Phys. Rev. Lett. **124**, 250402 (2020).
  - 29 Ananya Ghatak, Martin Brandenbourger, Jasper van Wezel, and Corentin Coulais, “Observation of non-Hermitian topology and its bulk-edge correspondence in an active mechanical metamaterial,” Proceedings of the National Academy of Sciences **117**, 29561–29568 (2020).
  - 30 Edan Lerner Martin Brandenbourger, Xander Locsin and Corentin Coulais, “Non-reciprocal robotic metamaterials,” Nat. Commun. **10**, 4608 (2019).
  - 31 Alexander B. Khanikaev Yakir Hadad, Jason C. Soric and Andrea Al, “Self-induced topological protection in nonlinear circuit arrays,” Nat. Electron. **1**, 178–182 (2018).
  - 32 Cui-Xian Guo, Chun-Hui Liu, Xiao-Ming Zhao, Yanxia Liu, and Shu Chen, “Exact solution of non-Hermitian systems with generalized boundary conditions: Size-dependent boundary effect and fragility of the skin effect,” Phys. Rev. Lett. **127**, 116801 (2021).
  - 33 Jia Ningyuan, Clai Owens, Ariel Sommer, David Schuster, and Jonathan Simon, “Time- and site-resolved dynamics in a topological circuit,” Phys. Rev. X **5**, 021031 (2015).
  - 34 Zhi-Qiang Zhang, Bing-Lan Wu, Juntao Song, and Hua Jiang, “Topological anderson insulator in electric circuits,” Phys. Rev. B **100**, 184202 (2019).
  - 35 Victor V. Albert, Leonid I. Glazman, and Liang Jiang, “Topological properties of linear circuit lattices,” Phys. Rev. Lett. **114**, 173902 (2015).
  - 36 Florian Bayer Johannes Brehm Laurens W. Molenkamp Tobias Kiessling Frank Schindler Ching Hua Lee Martin Greiter Titus Neupert Stefan Imhof, Christian Berger and Ronny Thomale, “Topoelectrical-circuit realization of topological corner modes,” Nat. Phys. **14**, 925929 (2018).
  - 37 Yuehui Lu, Ningyuan Jia, Lin Su, Clai Owens, Gediminas Juzeliūnas, David I. Schuster, and Jonathan Simon, “Probing the berry curvature and fermi arcs of a weyl circuit,” Phys. Rev. B **99**, 020302 (2019).
  - 38 Tobias Helbig, Tobias Hofmann, Ching Hua Lee, Ronny Thomale, Stefan Imhof, Laurens W. Molenkamp, and Tobias Kiessling, “Band structure engineering and reconstruction in electric circuit networks,” Phys. Rev. B **99**, 161114 (2019).
  - 39 Motohiko Ezawa, “Non-Hermitian boundary and interface states in nonreciprocal higher-order topological metals and electrical circuits,” Phys. Rev. B **99**, 121411.1–121411.5 (2019).
  - 40 Shuo Liu, Ruiwen Shao, Shaojie Ma, Lei Zhang, Oubo You, Haotian Wu, Yuan Jiang Xiang, Tie Jun Cui, and Shuang Zhang, “Non-Hermitian skin effect in a non-Hermitian electrical circuit,” Research **2021** (2021).
  - 41 S. Imhof M. Abdelghany T. Kiessling L. W. Molenkamp C. H. Lee A. Szameit M. Greiter T. Helbig, T. Hofmann and R. Thomale, “Generalized bulkboundary correspondence in non-Hermitian topoelectrical circuits,” Nat. Phys. **16**, 747 (2020).
  - 42 Farzad Zangeneh-Nejad and Romain Fleury, “Nonlinear second-order topological insulators,” Phys. Rev. Lett. **123**, 053902 (2019).
  - 43 Motohiko Ezawa, “Non-Hermitian higher-order topological states in nonreciprocal and reciprocal systems with their electric-circuit realization,” Phys. Rev. B **99** (2019).

- <sup>44</sup> Xiao-Xiao Zhang and Marcel Franz, “Non-Hermitian exceptional Landau quantization in electric circuits,” *Phys. Rev. Lett.* **124**, 046401 (2020).
- <sup>45</sup> Ke Xu, Xintong Zhang, Kaifa Luo, Rui Yu, Dan Li, and Hao Zhang, “Coexistence of topological edge states and skin effects in the non-Hermitian Su-Schrieffer-Heeger model with long-range nonreciprocal hopping in topoelectric realizations,” *Phys. Rev. B* **103**, 125411 (2021).
- <sup>46</sup> Shuo Liu, Shaojie Ma, Cheng Yang, Lei Zhang, Wenlong Gao, Yuan Jiang Xiang, Tie Jun Cui, and Shuang Zhang, “Gain- and loss-induced topological insulating phase in a non-Hermitian electrical circuit,” *Phys. Rev. Appl.* **13**, 014047 (2020).
- <sup>47</sup> Alexander Stegmaier, Stefan Imhof, Tobias Helbig, Tobias Hofmann, Ching Hua Lee, Mark Kremer, Alexander Fritzsche, Thorsten Feichtner, Sebastian Klemmt, Sven Höfling, Igor Boettcher, Ion Cosma Fulga, Libo Ma, Oliver G. Schmidt, Martin Greiter, Tobias Kiessling, Alexander Szameit, and Ronny Thomale, “Topological defect engineering and  $\mathcal{PT}$  symmetry in non-Hermitian electrical circuits,” *Phys. Rev. Lett.* **126**, 215302 (2021).
- <sup>48</sup> Naomichi Hatano and David R. Nelson, “Localization transitions in non-Hermitian quantum mechanics,” *Phys. Rev. Lett.* **77**, 570–573 (1996).
- <sup>49</sup> Naomichi Hatano and David R. Nelson, “Vortex pinning and non-Hermitian quantum mechanics,” *Phys. Rev. B* **56**, 8651–8673 (1997).
- <sup>50</sup> Philip W Anderson, “Absence of diffusion in certain random lattices,” *Phys. Rev.* **109**, 1492 (1958).
- <sup>51</sup> Although the Anderson localization is originally referred as the localization induced by the random disorder, in some references people also called the localization phenomena induced by quasiperiodic potentials as Anderson localization. Here we call both localization induced by random and quasiperiodic potentials as Anderson localization.
- <sup>52</sup> Hui Jiang, Li-Jun Lang, Chao Yang, Shi-Liang Zhu, and Shu Chen, “Interplay of non-Hermitian skin effects and Anderson localization in nonreciprocal quasiperiodic lattices,” *Phys. Rev. B* **100**, 054301 (2019).
- <sup>53</sup> Yanxia Liu, Qi Zhou, and Shu Chen, “Localization transition, spectrum structure, and winding numbers for one-dimensional non-Hermitian quasicrystals,” *Phys. Rev. B* **104**, 024201 (2021).
- <sup>54</sup> Stefano Longhi, “Phase transitions in a non-Hermitian Aubry-André-Harper model,” *Phys. Rev. B* **103**, 054203 (2021).
- <sup>55</sup> Jahan Claes and Taylor L. Hughes, “Skin effect and winding number in disordered non-Hermitian systems,” *Phys. Rev. B* **103**, L140201 (2021).

## Appendix A NON-RECIPROCAL CIRCUITS DESIGN

For the  $n$ th site in Fig. 4, due to Kirchhoff’s law, the incoming current is equal to the outgoing current

$$i_n = i_{n+1} + i_c + i_l \quad (8)$$

Taking time derivative to the above equation, then we have:

$$\frac{di_n}{dt} = \frac{di_{n+1}}{dt} + \frac{di_c}{dt} + \frac{di_l}{dt}. \quad (9)$$

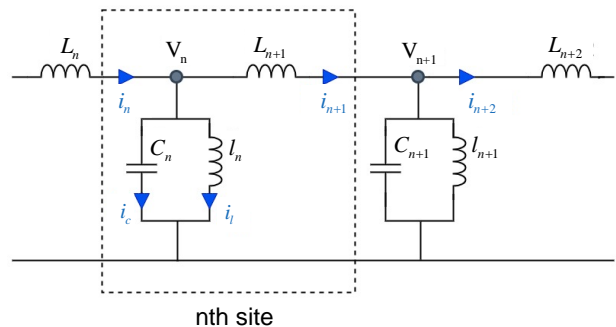


FIG. 4: Circuit diagram of two adjacent unit-cells.

With voltage-current characteristics of capacitance and inductance that

$$C \frac{dV}{dt} = i \text{ and } L \frac{di}{dt} = -V, \quad (10)$$

the Eq. (9) is hence replaced by

$$V_{n-1} + \frac{L_n}{L_{n+1}} V_{n+1} - \frac{L_n}{l_n} V_n = (L_n C_n \omega^2 + 1 + \frac{L_n}{L_{n+1}}) V_n \quad (11)$$

Here, we take  $g = L_n/L_{n+1}$  to represent the non-reciprocal hopping amplitude,  $\Delta_n = L_n/l_n$  is random on-site potential energy, the LC oscillator is characterized by its resonance frequency  $\omega$ , and  $\omega_0^2 = 1/L_n C_n = 1/LC$  denotes natural frequency. So, Kirchhoff’s law can be rewritten as<sup>52</sup>:

$$V_{n-1} + g V_{n+1} - \Delta_n V_n = (\omega^2/\omega_0^2 + 1 + g) V_n. \quad (12)$$

Consider all the voltages, written in matrix form  $H|V\rangle = E_n|V\rangle$ , so the  $n$ th eigenvalue  $E_n = \omega_n^2/\omega_0^2 + 1 + g$ . The form of the Eq. (12) is equivalent to the one-dimensional non-reciprocal competitive system constructed by us :

$$H = \sum_n |n+1\rangle\langle n| + g|n\rangle\langle n+1| + \Delta_n |n\rangle\langle n|. \quad (13)$$

Since each site is connected with an inductor to form  $\Delta_n$  to act as an Anderson disorder term. When  $\Delta_n = 2\Delta \cos(2\pi\beta n)$ , the model becomes a non-reciprocal AA model where  $\Delta$  is the amplitude of the quasiperiodic potential and  $\beta$  takes the value of the golden ratio  $(\sqrt{5} - 1)/2$ . For lack of on-site potential ( $\Delta_n = 0$ ), Eq. (13) translates to

$$H = \sum_n |n+1\rangle\langle n| + g|n\rangle\langle n+1|. \quad (14)$$

which denotes the HN model. Different skin states are formed according to  $g > 1$  ( $J_L > J_R$ ) or  $g < 1$  ( $J_L < J_R$ ).



## Appendix B EXPERIMENTAL IMPLEMENTATION

A circuit consisting of ten unit cells was realized on a PCB. The concise values for the circuit components are detailed in Tabs. I, II. The parameter error of the components is within 5%. In the implementation of the NHSE, we employ the chip capacitors, inductors and resistors. To reduce the influence of the inductors by the external magnetic field, we add a shielding cover to each inductor. We have made the same three circuit boards in each table.

To perform the spectral measurements, a constant a.c. voltage is fed into the beginning/last site of the board, while lock-in amplifiers are used to measure the each site's voltage response of the circuit separately. We use the transmission characteristics to get the resonance frequency. Three resonance frequencies are selected for each circuit board for measurement.

## Appendix C WINDING NUMBER

Topological winding number is defined as<sup>10</sup>:

$$\omega \equiv \int_{-\pi}^{\pi} \frac{dk}{2\pi i} \partial_k \ln(\det H(k)) \quad (15)$$

Let  $E_n(k)$  ( $n=1,2,\dots,N$ ) be the eigenenergy of  $H(k)$ , where  $N$  is the total number of bands. Then, Eq. (15) can be rewritten as:

$$\omega = \sum_{n=1}^N \int_{-\pi}^{\pi} \frac{dk}{2\pi} \partial_k \arg E_n(k), \quad (16)$$

where  $\arg E_n(k)$  is the argument of the complex energy  $E_n(k)$ . Therefore, for Hermitian Hamiltonians, the real energy implies  $\text{Arg} E_n(k) = 0, \pi$ .

We consider the HN model with asymmetric couplings as Eq. (7). By making Fourier transformation to moment space, so we obtain the Bloch Hamiltonian as:

$$H(k) = J_R e^{-ik} + J_L e^{ik}, \quad (17)$$

whose winding number is evaluated to give

$$\omega = \begin{cases} 1, & |J_R| < |J_L|, \\ -1, & |J_R| > |J_L|. \end{cases} \quad (18)$$

There is a topological phase transition as the winding number changes from 1 to -1. We note that  $\omega = 0$  when  $|J_R| = |J_L|$ .

TABLE I: Parameters of Fig. 2

subscript	Hermitian system (Fig. 2(d))			left-skin state (Fig. 2(e))		
	$L (\mu H)$	$C (nF)$	$R (\Omega)$	$L (\mu H)$	$C (nF)$	$R (\Omega)$
1	15	10	100	100	4.7	470
2	15	10	100	47	10	220
3	15	10	100	22	22	100
4	15	10	100	10	47	47
5	15	10	100	4.7	100	22
6	15	10	100	2.2	220	10
7	15	10	100	1	470	4.7
8	15	10	100	0.47	1000	2.2
9	15	10	100	0.22	2200	1
10	15	10	100	0.1	4700	0.47
11	15			0.047		

TABLE II: Parameters of Fig. 3

subscript	left-skin phase (Fig. 3(c))				Hermitian system (Fig. 3(d))				localized phase (Fig. 3(e))			
	$L (\mu H)$	$C (nF)$	$l (\mu H)$	$R (\Omega)$	$L (\mu H)$	$C (nF)$	$l (\mu H)$	$R (\Omega)$	$L (\mu H)$	$C (nF)$	$l (\mu H)$	$R (\Omega)$
1	33	1	100	1000	15	10	15	220	33	1	22	1000
2	15	2.2	220	470	15	10	15	220	15	2.2	2.2	470
3	6.8	4.7	150	220	15	10	15	220	6.8	4.7	0.68	220
4	3.3	10	330	100	15	10	15	220	3.3	10	33	100
5	1.5	22	330	47	15	10	15	220	1.5	22	0.15	47
6	0.68	47	470	22	15	10	15	220	0.68	47	0.15	22
7	0.33	100	220	10	15	10	15	220	0.33	100	0.1	10
8	0.15	220	100	4.7	15	10	15	220	0.15	220	0.012	4.7
9	0.068	470	150	2.2	15	10	15	220	0.068	470	0.15	2.2
10	0.033	1000	470	1	15	10	15	220	0.033	1000	0.0039	1
11	0.015				15				0.015			